Real-Time Observation of Carbonic Acid Formation in Aqueous Solution

Katrin Adamczyk, *et al.*

Science **326**, 1690 (2009);
DOI: 10.1126/science.1180060

the boundary without the need for dislocation slip events. In addition to acting as a direct mechanism for plastic flow, coupled grain boundary migration creates larger grains within the microstructure, which allows microscale plasticity mechanisms (normal dislocation plasticity) to become active (*8*).

Having pinpointed shear stress as the driving force governing mechanically induced grain growth, it is worth asking what role stress-driven grain boundary migration plays in governing materials behavior. The microstructural instability noted in nanocrystalline materials (*3*–*12*) indicates that grain boundary migration can result in mechanical behavior that is not only different from microcrystalline materials but dynamic as well. This departure from conventional plasticity is no doubt associated with the high stresses that nanocrystalline metals can accommodate. In conventional polycrystalline materials, the onset of dislocation-based plasticity limits the stresses that can be applied; nevertheless, it is reasonable to conclude that there may be hereto overlooked situations where stress-driven boundary migration influences the mechanical response and microstructural stability of other materials as well.

References and Notes

1. E. O. Hall, *Proc. Phys. Soc. B* **64**, 747 (1951).
2. N. J. Petch, *J. Iron Steel Inst. London* **174**, 25 (1953).
3. M. Jin, A. M. Minor, E. A. Stach, J. W. Morris Jr., *Acta Mater.* **52**, 5381 (2004).
4. M. Jin, A. M. Minor, J. W. Morris Jr., *Thin Solid Films* **515**, 3202 (2007).
5. K. Zhang, J. R. Weertman, J. A. Eastman, *Appl. Phys. Lett.* **87**, 061921 (2005).
6. D. Pan, S. Kuwano, T. Fujita, M. W. Chen, *Nano Lett.* **7**, 2108 (2007).
7. S. Brandstetter, K. Zhang, A. Escuadro, J. Weertman, H. Van Swygenhoven, *Scr. Mater.* **58**, 61 (2008).
8. D. S. Gianola *et al.*, *Acta Mater.* **54**, 2253 (2006).
9. G. J. Fan, L. F. Fu, H. Choo, P. K. Liaw, N. D. Browning, *Acta Mater.* **54**, 4781 (2006).
10. D. S. Gianola, D. H. Warner, J. F. Molinari, K. J. Hemker, *Scr. Mater.* **55**, 649 (2006).
11. D. S. Gianola, C. Eberl, X. M. Cheng, K. J. Hemker, *Adv. Mater.* **20**, 303 (2008).
12. M. Legros, D. S. Gianola, K. J. Hemker, *Acta Mater.* **56**, 3380 (2008).
13. J. W. Cahn, J. E. Taylor, *Acta Mater.* **52**, 4887 (2004).
14. J. W. Cahn, Y. Mishin, A. Suzuki, *Acta Mater.* **54**, 4953 (2006).
15. C. H. Li, E. H. Edwards, J. Washburn, E. R. Parker, *Acta Metall.* **1**, 223 (1953).
16. D. W. Bainbridge, C. H. Li, E. H. Edwards, *Acta Metall.* **2**, 322 (1954).
17. V. A. Ivanov, Y. Mishin, *Phys. Rev. B* **78**, 064106 (2008).
18. M. Winning, G. Gottstein, L. S. Shvindlerman, *Acta Mater.* **49**, 211 (2001).
19. M. Winning, G. Gottstein, L. S. Shvindlerman, *Acta Mater.* **50**, 353 (2002).
20. D. A. Molodov, V. A. Ivanov, G. Gottstein, *Acta Mater.* **55**, 1843 (2007).
21. D. L. Olmsted, E. A. Holm, S. M. Foiles, *Acta Mater.* **57**, 3694 (2009).
22. R. Ritchie, J. Knott, J. Rice, *J. Mech. Phys. Solids* **21**, 395 (1973).
23. R. K. Nalla, J. H. Kinney, R. O. Ritchie, *Nat. Mater.* **2**, 164 (2003).
24. V. Y. Gertsman, R. Birringer, *Scr. Metall. Mater.* **30**, 577 (1994).
25. J. Griffiths, D. Owen, *J. Mech. Phys. Solids* **19**, 419 (1971).
26. Materials and methods are available as supporting material on *Science* Online.
27. R. L. Coble, *J. Appl. Phys.* **34**, 1679 (1963).
28. G. Gottstein, L. S. Shvindlerman, *Grain Boundary Migration in Metals: Thermodynamics, Kinetics, Applications* (CRC, Boca Raton, FL, 1999).
29. M. F. Ashby, R. A. Verrall, *Acta Metall.* **21**, 149 (1973).
30. O. Sherby, J. Wadsworth, *Prog. Mater. Sci.* **33**, 169 (1989).
31. N. Bernstein, *Acta Mater.* **56**, 1106 (2008).
32. H. Zhang, D. Du, D. J. Srolovitz, *Philos. Mag.* **88**, 243 (2008).
33. F. Mompiou, D. Caillard, M. Legros, *Acta Mater.* **57**, 2198 (2009).
34. C. M. F. Rae, D. A. Smith, *Philos. Mag. A* **41**, 477 (1980).
35. D. Caillard, F. Mompiou, M. Legros, *Acta Mater.* **57**, 2390 (2009).

36. This work was supported by the U.S. Department of Energy, Office of Basic Energy Science and the NSF Nanoscale Interdisciplinary Research Team program (grant no. DMR-0210215). The authors are grateful for illuminating discussions with J. D. Embury and C. Eberl regarding the development of complex stress states in patterned thin films. D.S.G. acknowledges support from an Alexander von Humboldt postdoctoral fellowship.

Supporting Online Material

www.sciencemag.org/cgi/content/full/326/5960/1686/DC1
Materials and Methods
Figs. S1 and S2
Tables S1 and S2
References

25 June 2009; accepted 27 October 2009
10.1126/science.1178226

Real-Time Observation of Carbonic Acid Formation in Aqueous Solution

Katrin Adamczyk,[1] Mirabelle Prémont-Schwarz,[1] Dina Pines,[2] Ehud Pines,[2]* Erik T. J. Nibbering[1]*

Despite the widespread importance of aqueous bicarbonate chemistry, its conjugate acid, carbonic acid, has remained uncharacterized in solution. Here we report the generation of deuterated carbonic acid in deuterium oxide solution by ultrafast protonation of bicarbonate and its persistence for nanoseconds. We follow the reaction dynamics upon photoexcitation of a photoacid by monitoring infrared-active marker modes with femtosecond time resolution. By fitting a kinetic model to the experimental data, we directly obtain the on-contact proton-transfer rate to bicarbonate, previously inaccessible with the use of indirect methods. A Marcus free-energy correlation supports an associated pK_a (K_a is the acid dissociation constant) of 3.45 ± 0.15, which is substantially lower than the value of 6.35 that is commonly assumed on the basis of the overall carbon dioxide–to–bicarbonate equilibrium. This result should spur further exploration of acid-base reactivity in carbon dioxide–rich aqueous environments such as those anticipated under sequestration schemes.

Recent isolation of carbonic acid (H_2CO_3) in the gas and solid phases has conclusively disproved long-held claims of the molecule's intrinsic kinetic instability (*1*–*3*). Theoretical calculations have shown that H_2CO_3 only becomes unstable when water is present; that is, adding a single water molecule to anhydrous H_2CO_3 accelerates its simulated decomposition by a factor of 10^9 (*4*–*9*). Aqueous H_2CO_3 is understood to dissociate by a proton-relay mechanism that uses several catalyzing water molecules. For this reason, direct observation of aqueous H_2CO_3 has proven to be elusive, a situation that is somewhat surprising given the vital physiological role that the H_2CO_3/HCO_3^- buffer system has long been known to play in regulating the pH of blood and other biological fluids (*10*). Furthermore, sequestration plans to mitigate anthropogenic carbon dioxide emissions involve injecting several hundreds of gigatons of CO_2 into the oceans (*11*). Precise and reliable dissociation constants for carbonic acid over a wide range of ionic strengths, temperatures, and pressures will need to be established to determine in situ chemical behavior in such contexts (*12*–*14*).

In pure water (pH = 7 before CO_2 dissolution), aqueous solvation of CO_2 is understood to be accompanied by hydration, resulting in carbonic acid (H_2CO_3) (Eq. 1), and subsequent acid-base chemistry leading to bicarbonate (HCO_3^-) and carbonate (CO_3^{2-}) (Eq. 2)

$$CO_2(g) + 3H_2O \rightleftarrows CO_2(aq) + 3H_2O \rightleftarrows H_2CO_3 + 2H_2O \quad (1)$$

$$H_2CO_3 + 2H_2O \rightleftarrows HCO_3^- + H_3O^+ + H_2O \rightleftarrows CO_3^{2-} + 2H_3O^+ \quad (2)$$

The net result is a decrease in pH. Conversely, bicarbonate acts as a moderately weak base in solutions below neutral pH; titrations on time scales extending to minutes afford an effective pK_a (K_a is the acid dissociation constant) value

[1]Max Born Institut für Nichtlineare Optik und Kurzzeitspektroskopie, Max Born Strasse 2A, D-12489 Berlin, Germany. [2]Department of Chemistry, Ben-Gurion University of the Negev, Post Office Box 653, Beer-Sheva 84105, Israel.

*To whom correspondence should be addressed. E-mail: epines@bgu.ac.il (E.P.); nibberin@mbi-berlin.de (E.T.J.N.)

of 6.35, as represented by the reaction in Eq. 3 (*15*, *16*)

$$CO_2(aq) + 2H_2O \rightleftarrows HCO_3^- + H_3O^+ \quad (3)$$

It is important to note, however, that the nature of the conjugate acid $CO_2(aq)/H_2O$ is ill-defined, because the reactions in both Eqs. 1 and 2 participate in the chemistry. The true pK_a of carbonic acid would characterize the first equilibrium of Eq. 2, independent of the (de)hydration and (de)solvation reactions in Eq. 1. The value of the true acid dissociation constant of carbonic acid is connected to the effective value for $CO_2(aq)$ by the relation $K_a(H_2CO_3) = K_a(CO_2(aq)) \cdot (1 + [CO_2]/[H_2CO_3])$ (*15*) and may be found if the concentration ratio of CO_2 to H_2CO_3 is known. This ratio is usually assumed to have a value of several hundreds, implying concentrations of H_2CO_3 in water larger than 10^{-8} M, and $pK_a(H_2CO_3) \approx [pK_a(CO_2(aq)) - 2] \approx 4$. However, because the compound has so far eluded a direct detection, the true pK_a value and its associated implications for reactivity have been specified with large uncertainty (*16*, *17*).

Many earlier efforts to characterize the kinetics of aqueous carbonic acid have relied on indirect relaxation methods, including isotope exchange, temperature change, and pH-jump measurements, with limited temporal resolution (*18*, *19*). For example, determination of H_2CO_3 in time-resolved experiments by rapid mixing of $CO_2(aq)$ and a basic solution is difficult to achieve, because the kinetics of the forward reactions of Eq. 1 are dominated by the slowest step, namely hydration of $CO_2(aq)$ resulting in H_2CO_3. The ensuing dissociation of H_2CO_3 into H_3O^+ and HCO_3^- (Eq. 2) then leads to rapid depletion of H_2CO_3, precluding a substantial transient population build-up. The reverse reaction, involving transient protonation of HCO_3^-, could potentially lead to substantial generation of H_2CO_3. However, previous studies of the protonation reaction dynamics of HCO_3^- relied on stopped-flow techniques with insufficient time resolution for transient observation of the acid (*20*–*22*).

We overcame these challenges through the use of a photoacid that is optically triggered to transfer a proton to HCO_3^- on ultrafast time scales (Fig. 1). A photoacid exhibits a strong change in its pK_a value upon electronic excitation (*23*, *24*), enabling dynamical studies of processes with femtosecond time resolution, such as protonation of bases present in the same solution (*25*–*29*). We follow the progress of the photoinduced reaction by monitoring infrared (IR)–active marker modes of the photoacid, its conjugate photobase, and carbonic acid in D_2O. Solutions buffered at pD = 8 are used to prevent slow decomposition of DCO_3^- during the measurements. 2-Naphthol-6,8-disulfonate (2N-6,8S) is used as photoacid because it has the required properties (ground state $pK_a = 9.3$ to 9.4, excited state $pK_a = 1.0$ to 1.3 in D_2O at 0 M ionic strength) for excited-state deuteron transfer to DCO_3^- ($pK_a \approx 4$ for D_2CO_3). We optimized the working conditions (50 mM 2N-6,8S, 0.1 to 0.8 M DCO_3^-, 0.15 M TRIS/DCl as buffer dissolved in 100 ml solutions of D_2O) to ensure that changes in the solution caused by CO_2 loss remained moderate. To ensure that the changes did not affect the measured signal, we monitored the pD of the solution and the changes in relative concentration of photoacid and conjugate photobase before, during and after the measurements (figs. S1 and S3) (*19*).

Because we needed high concentrations (0.1 to 0.8 M) of the accepting base DCO_3^- to perform photoinduced diffusion-assisted bimolecular neutralization experiments, we were restricted to probing IR marker modes in spectral regions not rendered opaque by the DCO_3^- vibrational transitions, located at 1366 and 1628 cm^{-1} (Fig. 2A). The steady-state IR spectra of 2N-6,8S in the electronic ground state indicate that, throughout the fingerprint region, the vibrational mode patterns depend strongly on whether 2N-6,8S is in its photoacid or photobase configuration (Fig. 2B). In the transient pump-probe spectra, two spectrally resolved vibrational marker modes, with frequencies of 1472 and 1510 cm^{-1}, could be assigned, respectively, to the photoacid and photobase configurations of 2N-6,8S in its first electronic excited state (Fig. 2C). As a result, it was possible to monitor the decay of the 1472-cm^{-1} photoacid band and the corresponding rise of the photobase band at 1510 cm^{-1} as an unambiguous probe of the primary event of deuteron transfer, when 2N-6,8S releases its deuteron to either the solvent or to an accepting base (Fig. 2D). The 1410-cm^{-1} photobase band appeared to overlap spectrally with a carbonic acid band and, thus, could not be used to derive deuteron-transfer dynamics.

In addition, we observed the rise of a band at 1720 cm^{-1}, well within the frequency range where carbonyl stretching modes typically appear. This band position is in full accordance with the frequencies ranging from 1705 to 1730 cm^{-1} that have been reported in the literature on carbonic acid formed by high-energy irradiation of CO_2/water-ice mixtures (*30*–*32*), by proton irradiation of pure solid CO_2 or CO_2/water-ice mixtures (*31*, *32*), in protonated HCO_3^- embedded in ice matrices (*2*), on calcium carbonate surfaces reacting with SO_2 or HNO_3 in the presence of water (*33*), and with theoretical calculations (*34*). Theoretical results suggest that the vibrational bands observed in the solid and gas phase are actually due to H_2CO_3 dimers (*35*). Under our experimental conditions, involv-

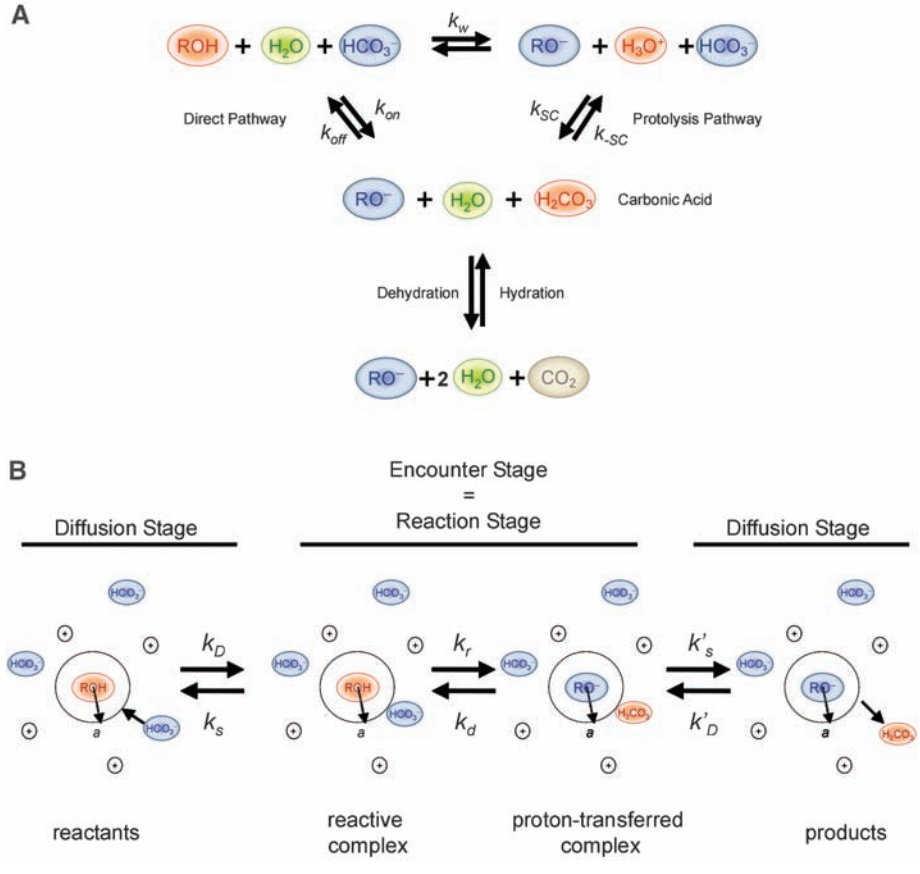

Fig. 1. (**A**) Reaction pathways between an organic acid and bicarbonate adapted from Eigen's scheme for acid-base neutralization (*22*). The hydrolysis and hydroxide addition pathways are omitted here for greater clarity, as these do not play a major role under our experimental conditions. (**B**) The diffusion and reaction stages of the direct pathway, explicitly taken into account in our diffusion-assisted bimolecular proton-transfer modeling. The reaction pair encounter distance is indicated with the symbol *a*.

ing ultrafast protonation of a base diluted in a polar solvent (D_2O), such dimers are not expected to be prominent. Based on the fact that we detect a product species with a vibrational marker mode located at a frequency typical for carbonyl stretching, we can exclude the generation of a zwitterionic structure (i.e., D_2O^+-COO^-) that could not be excluded as a potential intermediate in previous time-resolved studies of bicarbonate dehydration (*20*). Furthermore, in an experiment with 0.1 M DCO_3^-, we have been able to observe a correlation between the DCO_3^- marker-band decay and the D_2CO_3 marker-band rise, from which we ascertain that the D_2CO_3 marker band is an unequivocal probe for the final deuteron transfer to the accepting base (Fig. 3). We also performed two experiments using either $D^{12}CO_3^-$ or $D^{13}CO_3^-$ as accepting bases under identical conditions. We detected a frequency shift of the rising marker mode that matches known values for isotope shifts when comparing the C=O stretching mode of $D_2{}^{12}CO_3$ with that of $D_2{}^{13}CO_3$ (*36*, *37*). In addition, the ratio of the magnitude of DCO_3^- bleach and D_2CO_3 signal is in full accordance with reported values (*2*), indicating that the quantity of D_2CO_3 produced corresponds to the quantity of DCO_3^- lost.

We did not detect any transient signals in the region around 2364 cm^{-1} where the asymmetric stretching marker mode of CO_2 appears; thus, no substantial dehydration of D_2CO_3 to CO_2 occurs on subnanosecond time scales. Instead, D_2CO_3 appears to be a kinetically stable compound with a lifetime extending well beyond 1 ns, the maximum scanning range of our delay stage.

In the concentration range employed (0.1 to 0.8 M $NaDCO_3$; the maximum concentration that can be achieved for the buffered solutions, which have ionic strengths similar to that found in the oceans), neither the rise of the photobase marker band at 1510 cm^{-1} nor the rise of the D_2CO_3 marker band at 1720 cm^{-1} showed time-resolution–limited dynamics. Hence, we can exclude a prompt deuteron transfer away from the electronically excited photoacid, as well as subpicosecond deuteron transfer to the base. Previous results obtained for deuteron transfer from pyranine [8-hydroxy-pyrene-1,3,6-trisulfonate (HPTS)] to a family of carboxylate bases showed kinetics driven by a substantial fraction of on-contact reactive complexes, in which the photoacid and the base are directly linked, or else bridged by only a single water molecule (*26*–*28*). However, it appears here that on-contact reactive complexes, present at the moment of electronic excitation of the photoacid, are of minor importance. This may be because much lower concentrations were used in the present experiment on account of the lower solubility of sodium bicarbonate. Moreover, the relatively slow effective deuteron transfer could be a strong indication that in the acid-base neutralization of 2N-6,8S and DCO_3^-, the reactive encounter complex probably contains several water solva-

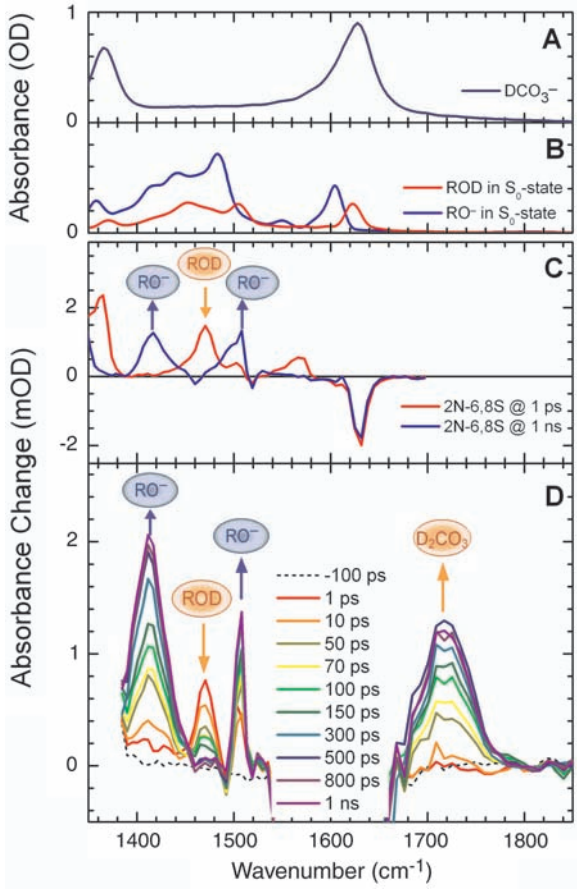

Fig. 2. (**A**) Experimental steady-state IR spectrum of $NaDCO_3$ in D_2O. (**B**) Steady-state IR spectra of 2N-6,8S in D_2O at pD = 1 (red curve) and pD = 12 (blue curve) showing the fingerprint modes of electronic ground state 2N-6,8S in the photoacid (ROD) and photobase (RO^-) forms, respectively. (**C**) Transient IR difference spectra measured for 2N-6,8S at pD = 5 in ROD form at a pulse delay of 1 ps (red curve) and after conversion into the RO^- form at a pulse delay of 1 ns (blue curve), showing bleach signals of fingerprint vibrations of ROD in the ground state and positive absorbance signals marking vibrations in the electronically excited state for both the ROD and RO^- forms. (**D**) Transient IR spectra of the neutralization reaction between 2N-6,8S and 0.5 M DCO_3^- measured at the probe pulse delays indicated in the legend, showing the marker modes of electronically excited 2N-6,8S in the ROD (1472 cm^{-1}) and RO^- (1410 and 1510 cm^{-1}) forms and of D_2CO_3 at 1720 cm^{-1}. OD, optical density.

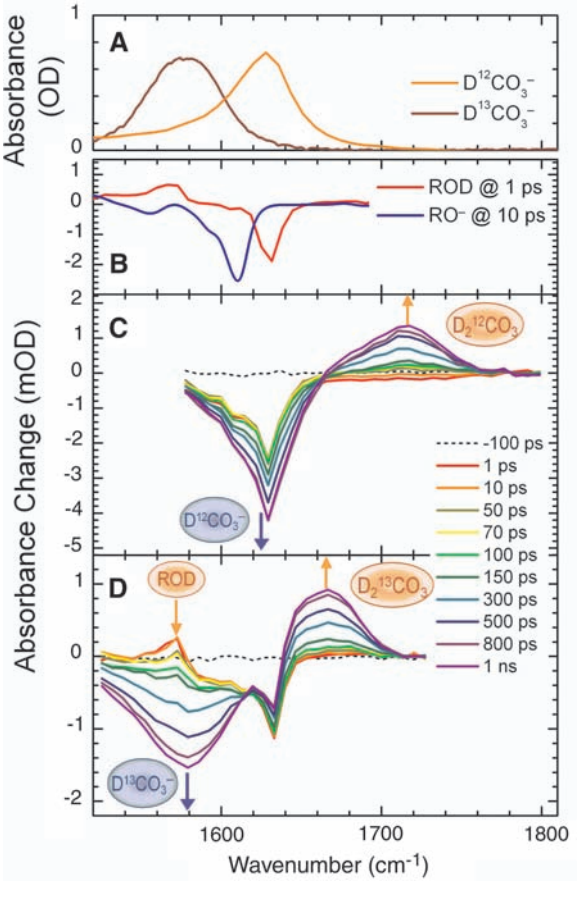

Fig. 3. (**A**) Steady-state IR spectrum of $D^{12}CO_3^-$ and $D^{13}CO_3^-$. (**B**) Transient IR difference spectrum of electronically excited 2N-6,8S in ROD (red curve) and RO^- (blue curve) forms, together with bleach signals corresponding to the ROD (1632 cm^{-1}) or RO^- species in the electronic ground state, generated within instrument-limited temporal resolution. (**C**) Kinetic measurement using 0.1 M $D^{12}CO_3^-$ showing the correlated bleach increase at the $D^{12}CO_3^-$ marker mode (1628 cm^{-1}) and the rise of the $D_2{}^{12}CO_3$ C=O stretching marker band (1720 cm^{-1}). (**D**) Kinetic measurement using 0.1 M $D^{13}CO_3^-$ showing the correlated bleach increase at the $D^{13}CO_3^-$ marker-mode frequency (1579 cm^{-1}) and the rise of the $D_2{}^{13}CO_3$ C=O stretching marker band (1666 cm^{-1}).

tion shells separating acid and base, whereas the proton transfer occurs on picosecond time scales. Similar results were obtained in a recent study of the acid-base neutralization of 2N-6,8S with cyanate performed with comparable base concentrations (*19*).

We have analyzed the transient spectra (Fig. 2D) recorded for three concentrations of DCO_3^- using a line-shape fitting routine to extract the kinetics of the vibrational marker bands (*19*). Briefly, bleach signals indicating marker bands of the photoacid or photobase in the S_0 state show no dynamics on the time scale of the experiment. Marker bands of the photoacid in the S_1 state decay with identical temporal characteristics to those with which the marker bands of the photobase in the S_1 state increase in magnitude. These two types of marker bands indicate the event of deuteron release from the photoacid (converting into the photobase) to possible accepting water solvent molecules (protolysis pathway of Fig. 1) or to the bicarbonate base (direct proton-transfer pathway of Fig. 1). The delayed deepening of the DCO_3^- bleach and the rise of the D_2CO_3 marker bands indicate binding of the deuteron at the base. The slower dynamics of these marker bands compared with those of the photoacid/photobase bands are a signature of deuterons temporarily residing on water (*26*, *27*). In Fig. 4, we display the time-dependent decay of the photoacid 1472 cm^{-1} band and the rise of the photobase band at 1510 cm^{-1} and of the carbonyl stretching band of D_2CO_3 at 1720 cm^{-1}. The nonexponential growth behavior of these latter marker bands, as well as the decay of the photoacid band at 1472 cm^{-1}, is governed by the time-dependent concentration gradient of the DCO_3^- base around the photoacid, which approaches a steady-state value at long times. The early time components are due to the reaction of 2N-6,8S with DCO_3^- in close proximity, involving minimal earlier mutual diffusion of the two reaction partners (*38*). The signals at longer pulse delays are due to acid and base reacting after substantial molecular diffusion toward each other. We have used an analytical framework derived by Szabo (see Fig. 1B) to describe the diffusion-controlled (time-dependent) reaction dynamics between 2N-6,8S and DCO_3^- under finite ionic strength (*19*, *39*). The resulting simulated reaction kinetics fit to the spectroscopic data are shown as solid lines in Fig. 4.

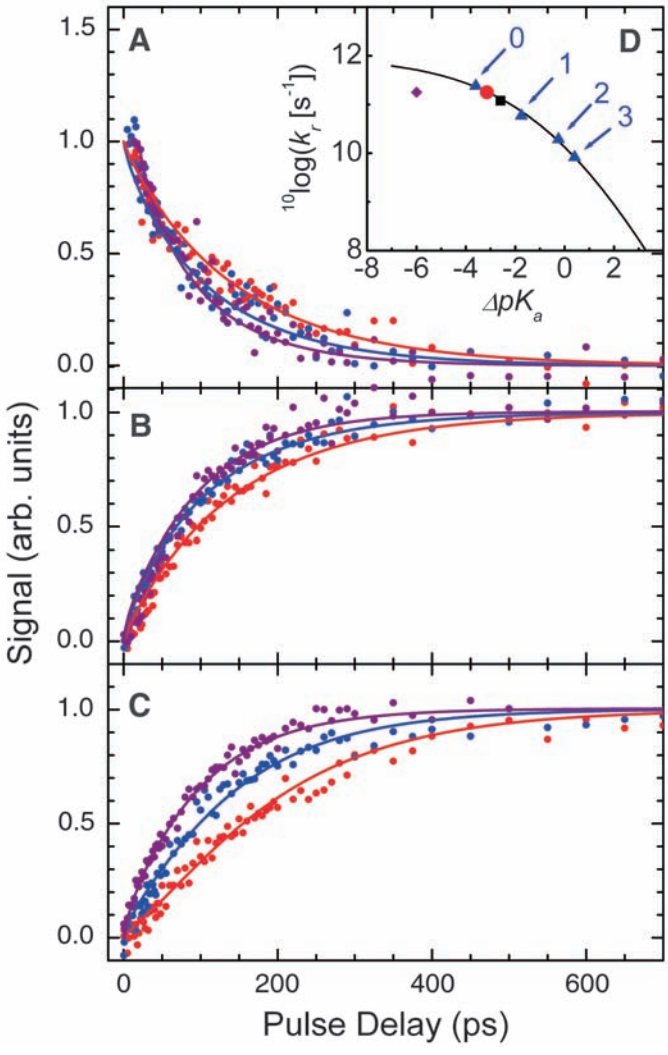

Fig. 4. Kinetics of the photoacid marker mode at 1472 cm^{-1} (**A**), the photobase transition at 1510 cm^{-1} (**B**), and the D_2CO_3 carbonyl stretching vibration at 1720 cm^{-1} (**C**) for three concentrations of DCO_3^- base: (i) 0.25 M (red dots), (ii) 0.5 M (blue dots), and (iii) 0.8 M (purple dots). Solid lines are fits with the use of the diffusion-assisted bimolecular reaction model described in the text. The free-energy correlation connecting ΔpK_a (acid-base) to the overall proton transfer in the encounter complex k_r is shown in (**D**). Blue triangles denote the acid-base neutralization reactions between HPTS and $CH_{3-x}Cl_xCOO^-$ (x = 0 to 3, as indicated with arrows), the black square indicates the reaction between HPTS and $HCOO^-$, the red dot denotes the reaction between 2N-6,8S and bicarbonate described here using a pK_a value of 3.45. For comparison, the purple diamond indicates where the point would appear using the effective pK_a value of 6.35.

We extract from the simulations a deuteron-transfer time of 8.6 ps upon formation of photoacid-base encounter complexes, implying even shorter times for proton transfer. The ultrafast proton-transfer rate $k_r = (6\ ps)^{-1} = 1.7 \cdot 10^{11}\ s^{-1}$ is about five times faster than the overall diffusion-limited rate constant that is calculated with similar values for the ionic strength. Thus, in a real-time experiment, we uncover details of the reaction dynamics that are unattainable with the experimental methods previously reported (*19*). In particular, a bimolecular (time-independent) rate constant of $k_{on} = 4.7 \cdot 10^{10}\ M^{-1}\ s^{-1}$ for the proton transfer to bicarbonate was reported by Eigen *et al.* with the use of indirect relaxation techniques (*20*, *22*). The measured reaction rate was found to be diffusion-limited, in accordance with our findings on the ultrafast (albeit finite) reaction rate of the encounter complex. In Fig. 4D, we compare the first-order protonation rate k_r in the encounter complex with previously reported results obtained from acid-base neutralization experiments of HPTS by carboxylate bases (*26*–*28*, *40*). We used the Marcus free-energy correlation for aqueous proton transfer (*19*, *41*) to plot the overall proton-transfer rate of the encounter complex as a function of ΔpK_a, defined as the difference between pK_a(photoacid in S_1 state) and pK_a (conjugate acid of accepting base). After correcting our measured rate for D/H isotope substitution (*19*), we found that the correlation holds for a carbonic acid pK_a of 3.45 ± 0.15, as opposed to the widely used effective pK_a of 6.35 for CO_2(aq)/H_2O. This result follows naturally from the real-time observation of proton transfer to bicarbonate on the picosecond time scale, without interfering effects from slower reversible deprotonation or dehydration reactions of carbonic acid.

Our work has clearly demonstrated that, in aqueous solution, D_2CO_3 is kinetically stable compared with its formation rate and that the dehydration rate of D_2CO_3 is relatively slow. Taking into account the combined effects of mutual diffusion (with forward k_D and backward k_s diffusion-controlled rates, respectively) and the proton transfer within the encounter complex (with forward k_r and backward k_d on-contact rates, respectively) (*38*), the deprotonation reaction rate constant (k_{off}) of D_2CO_3 (and, hence, the effective lifetime of the acid) at room temperature may be estimated from the measured overall deuteration rate of DCO_3^- anion, scaled to zero ionic strength, and the equilibrium acid dissociation constant of D_2CO_3: $k_{off} = K_a \cdot k_{on} = 10^{-pKa}\ M \cdot k_D k_r/(k_s + k_r)\ M^{-1}\ s^{-1} = 10^{-4}\ M \cdot 3.3 \cdot 10^{10}\ M^{-1}\ s^{-1} = 3.3 \times 10^6\ s^{-1}$. Here we have used the relation $pK_a(D_2CO_3) \approx pK_a(H_2CO_3) + 0.5$ (*15*). This rate constant corresponds to a lifetime of ~300 ns for D_2CO_3 before deuteron dissociation ensues. Therefore, from a kinetic point of view, the main cause of instability of D_2CO_3 over short times under aqueous conditions is acid

dissociation (deprotonation), rather than decomposition into CO_2 and H_2O, which takes place with an effective rate constant of $1.8 \cdot 10^1$ s^{-1} (*18*). This conclusion also holds for H_2CO_3, though the opposite is still commonly asserted by chemistry textbooks (*5*, *42*). Carbonic acid acts like an ordinary carboxylic acid on nanosecond time scales with an acidity comparable to that of formic acid. This considerable acidity of carbonic acid should henceforth be considered in the context of CO_2-rich aqueous environments. In particular, potential surface and deep-sea interfacial chemical reactivity of intact H_2CO_3 with solid substrates remains uncharted.

By comparing the magnitude of the D_2CO_3 signal at long pulse delays with the DCO_3^- bleach signal and using the known value for the extinction coefficient of DCO_3^- (933.5 M^{-1} cm^{-1}), we can derive a cross section of 750 ± 50 M^{-1} cm^{-1} for the C=O stretching mode of aqueous carbonic acid, which is comparable to that of carboxylic acids. This cross section should be sufficient to facilitate time-resolved IR studies of carbonic acid generation, deprotonation, and dehydration dynamics in biophysical systems. Probing the reaction dynamics of Eqs. 1 and 2 in the forward and backward directions as a function of ionic strength, temperature, and pressure will help in the determination of the reaction equilibrium constants under conditions that are relevant for the global carbon cycle.

References and Notes

1. J. K. Terlouw, C. B. Lebrilla, H. Schwarz, *Angew. Chem. Int. Ed. Engl.* **26**, 354 (1987).
2. W. Hage, K. R. Liedl, A. Hallbrucker, E. Mayer, *Science* **279**, 1332 (1998).
3. Historically, CO_2 has often been denoted as "carbonic acid," and H_2CO_3 was called "acid of air" or "aerial acid"; the correct IUPAC name for H_2CO_3 is "dihydrogencarbonate."
4. M. T. Nguyen, G. Raspoet, L. G. Vanquickenborne, P. T. Van Duijnen, *J. Phys. Chem. A* **101**, 7379 (1997).
5. T. Loerting *et al*., *Angew. Chem. Int. Ed.* **39**, 891 (2000).
6. C. S. Tautermann *et al*., *Chem. Eur. J.* **8**, 66 (2002).
7. M. Lewis, R. Glaser, *J. Phys. Chem. A* **107**, 6814 (2003).
8. P. P. Kumar, A. G. Kalinichev, R. J. Kirkpatrick, *J. Chem. Phys.* **126**, 204315 (2007).
9. M. T. Nguyen *et al*., *J. Phys. Chem. A* **112**, 10386 (2008).
10. I. Kurtz, J. Kraut, V. Ornekian, M. K. Nguyen, *Am. J. Physiol. Renal Physiol.* **294**, F1009 (2008).
11. B. Metz, O. Davidson, H. de Coninck, M. Loos, L. Meyer, Eds., *Working Group III of the Intergovernmental Panel on Climate Change: IPCC Special Report on Carbon Dioxide Capture and Storage* (Cambridge Univ. Press, Cambridge, 2005).
12. L. R. Kump, S. L. Brantley, M. A. Arthur, *Annu. Rev. Earth Planet. Sci.* **28**, 611 (2000).
13. P. Falkowski *et al*., *Science* **290**, 291 (2000).
14. F. J. Millero, *Chem. Rev.* **107**, 308 (2007).
15. R. P. Bell, *The Proton in Chemistry* (Chapman and Hall, London, ed. 2, 1973).
16. R. E. Zeebe, D. Wolf-Gladrow, *CO_2 in Seawater: Equilibrium, Kinetics, Isotopes*, Elsevier Oceanography Series 65 (Elsevier, Amsterdam, Netherlands, 2001).
17. K. F. Wissbrun, D. M. French, A. Patterson Jr., *J. Phys. Chem.* **58**, 693 (1954).
18. Y. Pocker, D. W. Bjorkquist, *J. Am. Chem. Soc.* **99**, 6537 (1977).
19. For further details, see the supporting material available on *Science* Online.
20. M. Eigen, K. Kustin, G. Maass, *Z. Phys. Chem. N. F.* **30**, 130 (1961).
21. The citation in reference (*20*) discusses the protolytic conversion dynamics of bisulfite to sulfur dioxide, with reaction pathways similar to those of carbon dioxide. Reaction rates are given for both bisulfite and bicarbonate.
22. M. Eigen, *Angew. Chem. Int. Ed. Engl.* **3**, 1 (1964).
23. E. Pines, D. Huppert, *J. Phys. Chem.* **87**, 4471 (1983).
24. L. M. Tolbert, K. M. Solntsev, *Acc. Chem. Res.* **35**, 19 (2002).
25. L. Genosar, B. Cohen, D. Huppert, *J. Phys. Chem. A* **104**, 6689 (2000).
26. M. Rini, B.-Z. Magnes, E. Pines, E. T. J. Nibbering, *Science* **301**, 349 (2003).
27. O. F. Mohammed, D. Pines, J. Dreyer, E. Pines, E. T. J. Nibbering, *Science* **310**, 83 (2005).
28. O. F. Mohammed, D. Pines, E. T. J. Nibbering, E. Pines, *Angew. Chem. Int. Ed.* **46**, 1458 (2007).
29. M. J. Cox, H. J. Bakker, *J. Chem. Phys.* **128**, 174501 (2008).
30. M. H. Moore, R. K. Khanna, *Spectrochim. Acta A* **47**, 255 (1991).
31. J. R. Brucato, M. E. Palumbo, G. Strazzulla, *Icarus* **125**, 135 (1997).
32. P. A. Gerakines, M. H. Moore, R. L. Hudson, *Astron. Astrophys.* **357**, 793 (2000).
33. H. A. Al-Hosney, V. H. Grassian, *J. Am. Chem. Soc.* **126**, 8068 (2004).
34. C. A. Wight, A. I. Boldyrev, *J. Phys. Chem.* **99**, 12125 (1995).
35. J. A. Tossell, *Inorg. Chem.* **45**, 5961 (2006).
36. W. Hage, A. Hallbrucker, E. Mayer, *J. Chem. Soc. Faraday Trans.* **92**, 3183 (1996).
37. W. Hage, A. Hallbrucker, E. Mayer, *J. Chem. Soc. Faraday Trans.* **92**, 3197 (1996).
38. E. Pines, B. Z. Magnes, M. J. Lang, G. R. Fleming, *Chem. Phys. Lett.* **281**, 413 (1997).
39. A. Szabo, *J. Phys. Chem.* **93**, 6929 (1989).
40. O. F. Mohammed, D. Pines, E. Pines, E. T. J. Nibbering, *Chem. Phys.* **341**, 240 (2007).
41. A. O. Cohen, R. A. Marcus, *J. Phys. Chem.* **72**, 4249 (1968).
42. R. Ludwig, A. Kornath, *Angew. Chem. Int. Ed.* **39**, 1421 (2000).

43. This work was supported by the German-Israeli Foundation for Scientific Research and Development (grant GIF I-876-107.5 to E.T.J.N. and E.P.) and the James Franck German-Israel Binational Program in Laser-Matter Interaction (E.P.). We thank L. M. Tolbert for suggesting that we delve into the subject of carbonic acid.

Supporting Online Material

www.sciencemag.org/cgi/content/full/1180060/DC1
SOM Text
Figs. S1 to S5
Table S1
References

3 August 2009; accepted 20 October 2009
Published online 12 November 2009;
10.1126/science.1180060
Include this information when citing this paper.

Bacterial Community Variation in Human Body Habitats Across Space and Time

Elizabeth K. Costello,[1] Christian L. Lauber,[2] Micah Hamady,[3] Noah Fierer,[2,4] Jeffrey I. Gordon,[5] Rob Knight[1,6]*

Elucidating the biogeography of bacterial communities on the human body is critical for establishing healthy baselines from which to detect differences associated with diseases. To obtain an integrated view of the spatial and temporal distribution of the human microbiota, we surveyed bacteria from up to 27 sites in seven to nine healthy adults on four occasions. We found that community composition was determined primarily by body habitat. Within habitats, interpersonal variability was high, whereas individuals exhibited minimal temporal variability. Several skin locations harbored more diverse communities than the gut and mouth, and skin locations differed in their community assembly patterns. These results indicate that our microbiota, although personalized, varies systematically across body habitats and time; such trends may ultimately reveal how microbiome changes cause or prevent disease.

The human body hosts complex microbial communities whose combined membership outnumbers our own cells by at least a factor of 10 (*1*, *2*). Together, our ~100 trillion microbial symbionts (the human microbiota) endow us with crucial traits; for example, we rely on them to aid in nutrition, resist pathogens, and educate our immune system (*1*, *3*). To understand the full range of human genetic and metabolic diversity, it is necessary to characterize the factors influencing the diversity and distribution of the human microbiota (*4*, *5*).

Determining our microbiota's role in disease predisposition and pathogenesis will depend critically upon first defining "normal" states (*5*). Prior studies of healthy individuals have focused on particular body habitats including the gut (*6*, *7*), skin (*8*–*10*), and oral cavity (*11*, *12*), and have revealed microbial communities that were highly variable both within

[1]Department of Chemistry and Biochemistry, University of Colorado, Boulder, CO 80309, USA. [2]Cooperative Institute for Research in Environmental Sciences, University of Colorado, Boulder, CO 80309, USA. [3]Department of Computer Science, University of Colorado, Boulder, CO 80309, USA. [4]Department of Ecology and Evolutionary Biology, University of Colorado, Boulder, CO 80309, USA. [5]Center for Genome Sciences, Washington University School of Medicine, St. Louis, MO 63108, USA. [6]Howard Hughes Medical Institute.

*To whom correspondence should be addressed. E-mail: rob.knight@colorado.edu